ELECTROCATALYSIS

Direct propylene epoxidation via water activation over Pd-Pt electrocatalysts

Minju Chung[1], Joseph H. Maalouf[1], Jason S. Adams[2], Chenyu Jiang[2], Yuriy Román-Leshkov[1], Karthish Manthiram[2]*

Direct electrochemical propylene epoxidation by means of water-oxidation intermediates presents a sustainable alternative to existing routes that involve hazardous chlorine or peroxide reagents. We report an oxidized palladium-platinum alloy catalyst ($PdPtO_x$/C), which reaches a Faradaic efficiency of 66 ± 5% toward propylene epoxidation at 50 milliamperes per square centimeter at ambient temperature and pressure. Embedding platinum into the palladium oxide crystal structure stabilized oxidized platinum species, resulting in improved catalyst performance. The reaction kinetics suggest that epoxidation on $PdPtO_x$/C proceeds through electrophilic attack by metal-bound peroxo intermediates. This work demonstrates an effective strategy for selective electrochemical oxygen-atom transfer from water, without mediators, for diverse oxygenation reactions.

Propylene oxide (PO) is an important chemical building block used in the production of many commodity chemicals, such as polyurethanes and polyesters (*1*). Currently, PO production relies on highly reactive, corrosive, or explosive chemical oxidants such as molecular chlorine (Cl_2) or peroxides (*2*). Although direct oxidation of propylene with molecular oxygen (O_2) has been explored as an alternative solution, achieving high selectivity for PO is challenging because of the allylic hydrogen stripping in propylene and consequent further oxidation (*2*). In this regard, a selective direct propylene-epoxidation pathway that uses water as a cleaner and an easily accessible oxygen source would present a compelling alternative to the current epoxidation methods.

Electrochemistry offers a promising approach for using water as a sustainable source of oxygen atoms at ambient temperature and pressure. In water electrolysis, typically oxygen and hydrogen are generated, but alternatively, commodity chemicals can be synthesized through oxidative processes at the anode of an electrochemical cell combined with hydrogen evolution at the cathode. For example, chloride oxidation can be conducted at the anode to generate Cl_2, which acts as a redox mediator in alkene epoxidation (Fig. 1A, bottom) (*3*–*5*). This electrified version of the chlorohydrin process was demonstrated to be effective at industrially relevant current densities and selectivity (*4*). However, this method produces byproducts such as hypochlorite, chlorinated organic compounds, and brine streams that pose serious environmental challenges unless 100% selectivity and recycling of the chloride electrolytes can be achieved. Rather than relying on Cl_2 as a redox mediator, it should be possible to directly transfer reactive intermediates typically seen in water oxidation to the alkene before the intermediates are fully oxidized into O_2 (Fig. 1A, top) (*6*–*8*). This direct electrochemical alkene-epoxidation approach does not involve hazardous oxidizing agents, such as Cl_2, making it an attractive avenue for high-demand propylene epoxidation.

[1]Department of Chemical Engineering, Massachusetts Institute of Technology, Cambridge, MA 02139, USA.
[2]Division of Chemistry and Chemical Engineering, California Institute of Technology, Pasadena, CA 91125, USA.
*Corresponding author. Email: karthish@caltech.edu

Catalytic performance of $PdPtO_x$/C and design principle

Previously studied catalysts for electrochemical propylene epoxidation can be clustered into palladium-derived (Pd) (*9*–*12*), platinum-derived (Pt) (*13*–*15*), and silver-derived (Ag) (*16*, *17*) groups (Fig. 1B and table S1), and the best catalytic performance for electrochemical epoxidation has been observed with oxidized Pd and Pt catalysts. Studies on Pd catalysts have shown that epoxidation occurs on the surface oxide layer at anodic potentials >1.1 V versus reversible hydrogen electrode (RHE), whereas allylic oxidation producing acrolein and acrylic acid occurs on the metallic surface at lower potentials (*9*, *12*). The performance enhancement of oxidized Pt catalysts was correlated with an increase in surface presence of Pt(II) and Pt(IV) species, whereas pure PtO_2 was less active (*14*). Moreover, a theoretical study has identified weak oxygen-binding metal oxides as promising catalyst candidates for propylene epoxidation and cautioned that the metallic phase of strong-binding metals, such as Pt and Pd, may facilitate the production of unwanted side products through dehydrogenation (*18*). These findings suggest that the catalytic performance may be further optimized by adjusting the oxidation states of the metal. However, preparing Pt oxide catalysts with high concentrations of oxidized Pt species is challenging because of their instability. By contrast, stable Pd oxide catalysts can be obtained through high-temperature annealing, but they generally exhibit lower rates of epoxidation.

Alloying Pt with Pd can be a strategy that leverages complementary properties of the two elements, enabling the attainment of optimal oxidation states and structures for an epoxidation catalyst (Fig. 1C). Under aerobic conditions, Pt nanoparticles tend to sinter into a metallic form when annealed above 400°C (*19*) because volatile PtO_2 species mediate the sintering process by facilitating Ostwald ripening (*20*, *21*). By contrast, stable PdO nanoparticles can be produced through annealing of Pd nanoparticles without substantial sintering (*19*, *22*). PdO can trap mobile PtO_2 species, which results in less sintering of Pd-Pt alloy nanoparticles than of Pt nanoparticles (*20*, *23*). In addition, Pd and Pt share very similar crystal structures and atomic sizes, allowing homogeneous distributions of Pd and Pt in their alloys.

In this study, we designed a Pd-Pt alloy catalyst containing both Pd oxide and Pt oxide by embedding and stabilizing Pt oxide species in Pd oxide. A series of alloys with varying ratios of Pd and Pt were synthesized using a coreduction method (*24*) on an amorphous carbon substrate and subsequently annealed under static air before being tested for their activity in propylene epoxidation (materials and methods and figs. S1 to S3). Our catalyst is compatible with a blended electrolyte composed of acetonitrile and water (Fig. 1D) that can accommodate a broad spectrum of alkene substrates, as well as aqueous electrolytes (Fig. 1E) that can minimize overall cell voltage for gaseous-alkene epoxidation (fig. S4). The alloy catalyst with an equimolar composition of Pd and Pt annealed at 500°C ($PdPtO_x$/C) was most active toward propylene epoxidation and outperformed previously reported catalysts for direct anodic epoxidation under ambient conditions (Fig. 1B and table S1). Furthermore, alloys with metal compositions of Pd_3Pt_1 and Pd_1Pt_3 exhibited epoxidation activities on par with those of $PdPtO_x$/C; when Pd and Pt are mixed at the nanometer scale (figs. S2 and S3), Pd-Pt alloy catalysts can achieve enhanced epoxidation rates and Faradaic efficiencies (FEs) relative to either Pd or Pt alone (Fig. 1, D and E, and fig. S5).

In an electrolytic cell equipped with circulating liquid electrolytes (fig. S4), we demonstrated continuous PO production with high FE averaging 66 ± 5% [propylene glycol (PG); 1.3 ± 0.3%] for 3 hours at a constant current density of 50 mA/cm^2. Additionally, $PdPtO_x$/C catalyzed cyclooctene epoxidation with an FE of ~90%, a notable improvement over the results observed in our previous studies, in which we used Ir-MnO_x (~50%) and MnO_x (~30%) catalysts (table S2) (*7*, *8*).

Catalyst characterizations

We examined the bulk and surface properties of our annealed PdPt/C, Pd/C, and Pt/C catalysts ($PdPtO_x$/C, PdO_x/C, and PtO_x/C, respectively)

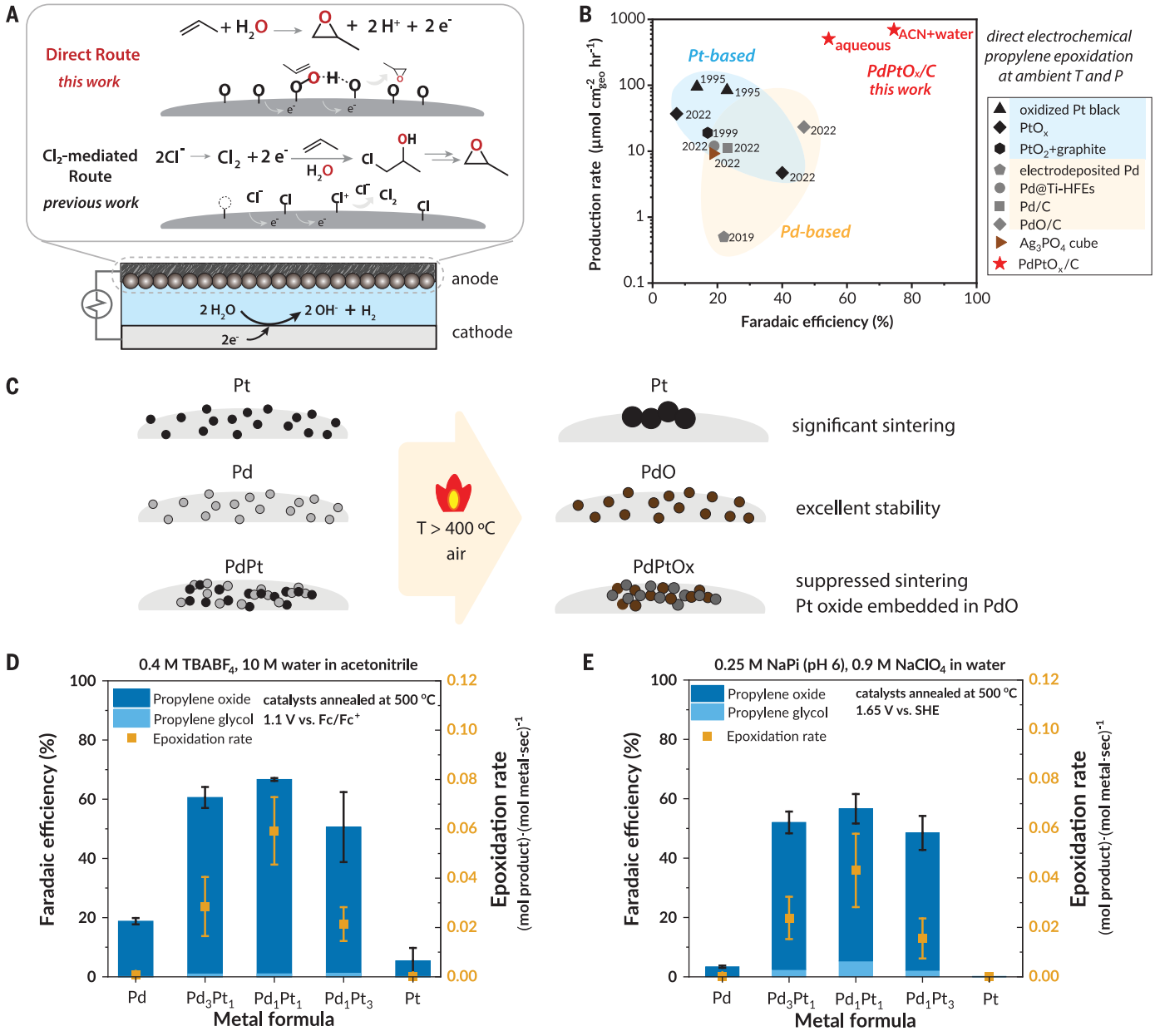

Fig. 1. Background and demonstration of direct electrochemical propylene epoxidation. (**A**) Comparison of chlorine-mediated and direct electrochemical propylene epoxidation. (**B**) Compilation of previously reported direct electrochemical propylene epoxidation and our work. (**C**) Effect of annealing on Pt, Pd, and Pd-Pt nanoparticles. (**D** and **E**) Direct electrochemical propylene-epoxidation performance with different compositions of Pd-Pt-on-carbon catalysts in (D) water-acetonitrile electrolyte and (E) aqueous electrolyte. Potentials in this figure were 100% iR-compensated (i, current; R, resistance). The vertical error bars represent standard deviations from the mean of multiple replicates (n = 3) of the same experiment.

to shed light on the enhanced performance of $PdPtO_x$/C compared with PdO_x/C and PtO_x/C.

X-ray diffraction (XRD) patterns showed that although PdO_x/C and PtO_x/C only exhibited oxide and metallic phases, respectively, the $PdPtO_x$/C contained both phases (Fig. 2A and fig. S6). The oxide phase of $PdPtO_x$/C resembles that of PdO_x/C because the (101) peak in $PdPtO_x$/C at 33.7° occurs at a similar angle as the PdO_x/C peak at 33.9°. Similarly, the metallic phase of $PdPtO_x$/C parallels that of PtO_x/C, with the (111) peak shifted from 39.8° in PtO_x/C to 40.0° in $PdPtO_x$/C. Furthermore, the broader peaks in the $PdPtO_x$/C XRD pattern indicate that the $PdPtO_x$/C has smaller crystallites than those of PtO_x/C (table S3), which is consistent with our hypothesis that the sintering of PdPt/C is less severe than that of Pt/C upon annealing.

Extended x-ray absorption fine structure (EXAFS) measurements revealed that, within fitting errors, Pd and Pt coordinate with the same number of oxygens in $PdPtO_x$/C; the Pd-O and Pt-O coordination numbers were estimated to be 3.7 ± 0.4 and 2.8 ± 0.6, respectively (Fig. 2, B and C, and tables S4 to S6). The local coordination environments of Pd in $PdPtO_x$/C and PdO_x/C were similar to that of PdO, whereas PtO_x/C resembled the Pt foil standard and did not show any contribution from the Pt-O scattering path. By contrast, the local environment of Pt in $PdPtO_x$/C was different from that in the Pt foil or PtO_2 standard, and the first-shell scattering path of $PdPtO_x$/C was fit with a combination of Pt-O and Pt-Pd/Pt scattering paths. These EXAFS data suggest that blending Pt in the PdO structure induced a local coordination

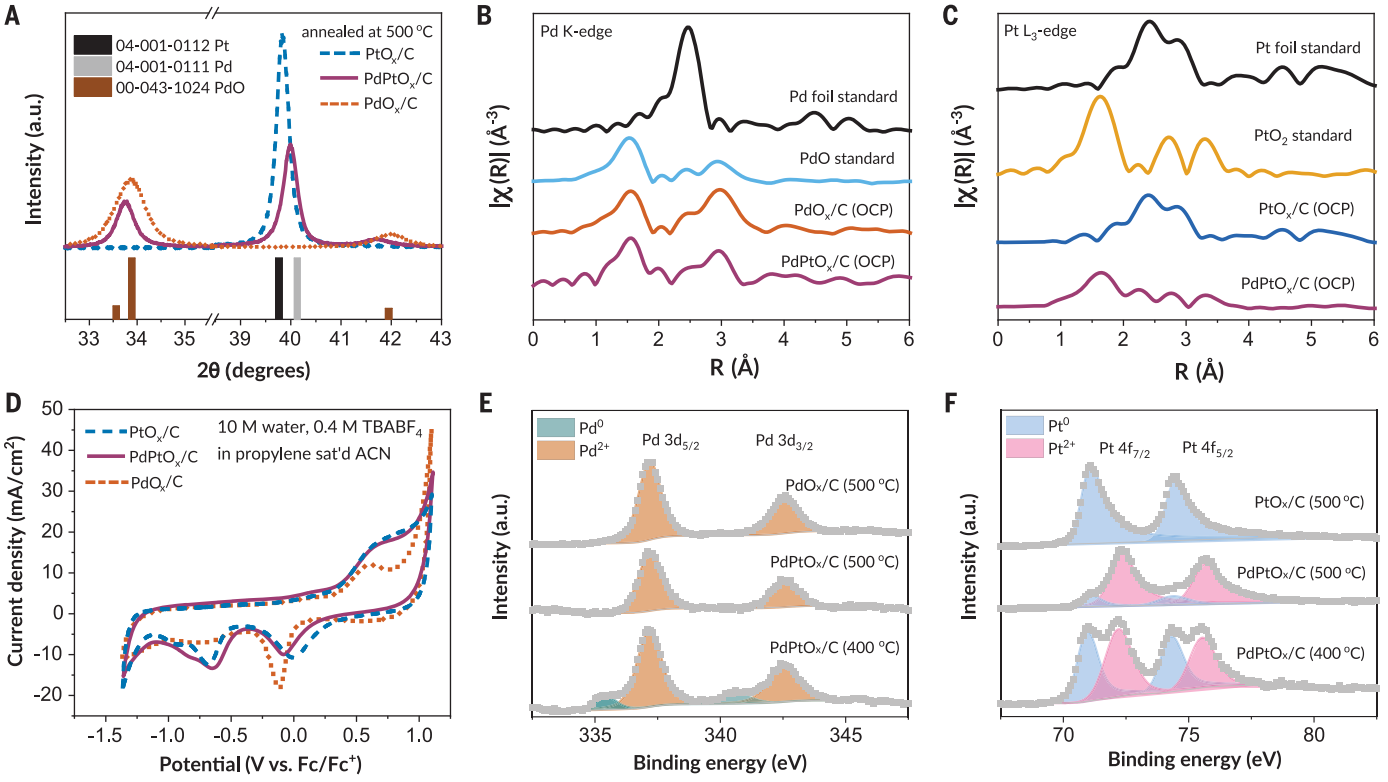

Fig. 2. Ex situ characterizations of annealed PdPt/C, Pd/C, and Pt/C catalysts. (**A**) Magnified XRD patterns around the peak associated with the oxide and metallic phases of annealed catalysts at 500°C. (**B** and **C**) EXAFS spectra of standards and catalysts at (B) Pd K-edge and (C) Pt L_3-edge. (**D**) Cyclic voltammetry traces of the catalysts. The scans were recorded at 50 mV/sec scan rate with 85% automatic iR compensation (i, current; R, resistance). (**E**) High-resolution Pd 3d XPS spectra of annealed Pd/C and PdPt/C catalysts. (**F**) High-resolution Pt 4f XPS spectra of annealed Pt/C and PdPt/C catalysts.

environment of Pt resembling that of PtO, which is unstable alone.

The mixing of Pd and Pt on the surface, matching the bulk composition, was confirmed through cyclic voltammetry (CV) and x-ray photoelectron spectroscopy (XPS) analyses. A single peak of surface-oxide reduction [at ~0 V versus ferrocene/ferrocenium (Fc/Fc^+)] was observed in the CV of the $PdPtO_x/C$ electrode, suggesting that Pd and Pt coexist on the catalyst surface (Fig. 2D and fig. S7). Furthermore, near-surface compositions derived from XPS survey spectra also indicate that Pd and Pt are present in an equimolar ratio near the surface (table S7), matching the bulk composition determined with inductively coupled plasma-optical emission spectrometry (table S8).

XPS analysis showed that alloying Pt with Pd stabilizes oxidized Pt on the catalyst surface. Pt(0) species were dominant in the PtO_x/C, whereas a higher content of Pt(II) species was observed in $PdPtO_x/C$ (Fig. 2F). The ratio of Pt(II):Pt(0) increased from 1.0 to 6.4 as the catalyst treatment temperature was increased from 400° to 500°C (table S9). A small amount of Pd(0) was present in $PdPtO_x/C$ annealed at 400°C, whereas Pd(II) was exclusively observed in the catalyst annealed at 500°C (Fig. 2E). The epoxidation rate and selectivity also improved with the treatment temperature for PdPt/C (figs. S8 and S9), indicating that the higher ratio of oxidized Pd and Pt species is contributing to the enhancement in the catalyst performance.

Operando x-ray absorption spectroscopy (XAS) experiments probing the Pd K-edge and Pt L_3-edges during epoxidation highlighted again that achieving more oxidized Pt may have a critical role in improving catalytic activity toward propylene epoxidation. Progressively more oxidative potentials were applied from 0.45 to 1.15 V versus Fc/Fc^+, followed by a reductive step to −1.35 V and then two oxidative steps back to 1.15 V. The average metal valency at each condition was estimated from linear combination fitting of x-ray absorption near edge structure (XANES) spectra by using reference spectra from standard materials. The results indicate that PdO stabilizes oxidized Pt species in Pd-Pt alloys, leading to a higher average oxidation state of Pt in $PdPtO_x/C$ (+2) compared with that in PtO_x/C (0). This difference is maintained under anodic potentials (0.45 to 1.15 V versus Fc/Fc^+, Fig. 3A). Unlike the stark contrast in Pt valency between $PdPtO_x/C$ and PtO_x/C, the Pd valency stayed the same (+2) in both $PdPtO_x/C$ and PdO_x/C (Fig. 3B). These observations suggest that the more-oxidized Pt species contribute to the enhancement in the production rate and selectivity of PO.

Furthermore, EXAFS fitting of catalysts under operating conditions showed that coordination numbers and scattering-path lengths of Pd and Pt did not change during electrolysis (tables S5 and S6). Applying a cathodic potential followed by an anodic potential demonstrated that the edge energies and the coordination environment of Pd and Pt respond to applied potentials in a partially, albeit not fully, reversible fashion (Fig. 3 and figs. S10 and S11).

The results from XRD, CV, and the elemental analysis collectively suggest that Pd and Pt are mixed in both the bulk and surface of the $PdPtO_x/C$ catalyst. XANES and XPS results revealed that a larger quantity of oxidized Pt species is stabilized in $PdPtO_x/C$ than in PtO_x/C. XAS data suggest that Pd stabilizes Pt at a similar oxidation state (around +2) and crystal structure as those of PdO, and these combined factors improve catalytic performance.

Electrochemical kinetic study and proposed reaction mechanism

Understanding the mechanism of direct propylene epoxidation on $PdPtO_x/C$ can help us develop more efficient catalysts and process conditions for producing PO. The reaction mechanism was investigated with a multifaceted approach, including kinetic rate measurements, deuterium kinetic isotope effect measurements,

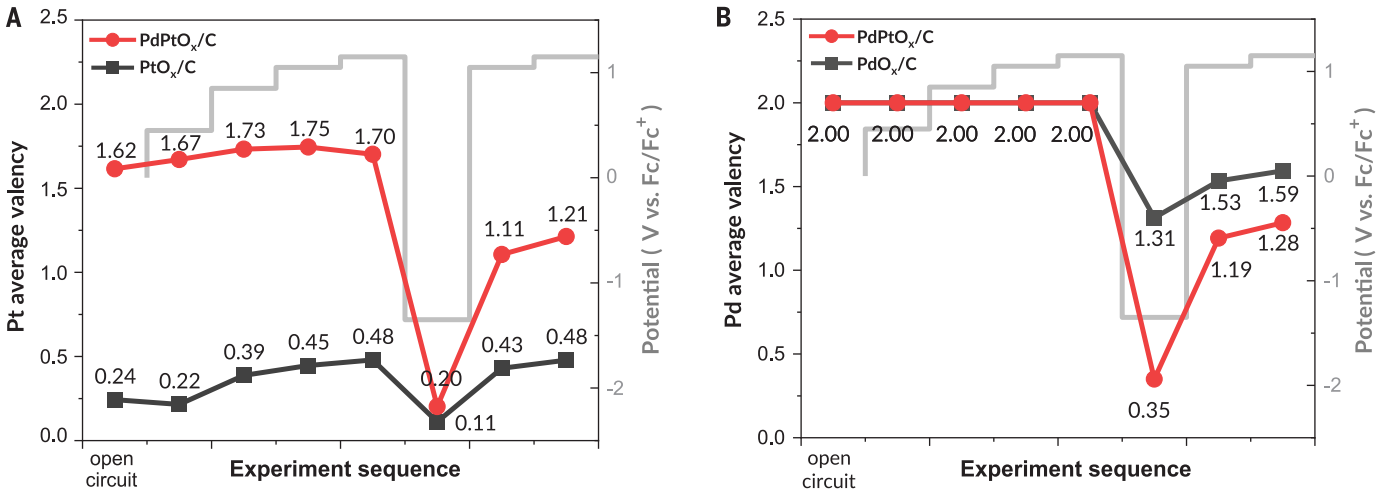

Fig. 3. Operando x-ray absorption spectroscopy. (**A**) Changes of Pt average valency in PdPtO$_x$/C and PtO$_x$/C in responses to applied potentials. (**B**) Changes of Pd average valency in PdPtO$_x$/C and PdO$_x$/C in responses to applied potentials. Potentials in this figure were 100% iR-compensated (i, current; R, resistance).

probe substrate analysis, and substrate-based descriptor assessment.

Electrochemical kinetic rate measurements were conducted to examine electrolyte species dependences for direct anodic epoxidation on PdPtO$_x$/C (Fig. 4 and figs. S12 and S13). The reaction rates, represented by the partial current density toward epoxidation, were measured with chronoamperometry in conjunction with product quantification performed with proton nuclear magnetic resonance (^{1}H-NMR) (materials and methods).

We hypothesized that the direct alkene-epoxidation pathway at the anode may involve multiple coupled proton-electron transfer steps from water to the electrode, followed by oxygen-atom transfer from intermediates typically seen in water oxidation to propylene. O_2 was observed to be the major byproduct with the PdPtO$_x$/C catalyst, although a small amount of CO_2 was also observed (fig. S14). It is worth noting that the selectivity of PO over other propylene-derived products (PG, acetone, and CO_2) reaches 92%. Therefore, in our proposed mechanism, only the competition between epoxidation and oxygen evolution was considered.

In cases in which the surface coverage is primarily determined by a single reactive intermediate and a rate-limiting step is evident, the measured Tafel slope of 119 ± 5 mV/decade implies that the rate-limiting step involves a single electron transfer and that no pre-equilibrated electron transfer steps occur between the abundant reactive intermediate and the rate-limiting step (Fig. 4A). Nevertheless, noninteger and nonlinear reaction orders were observed in the water and propylene dependences, signaling the presence of more intricate kinetic control.

At 1 atm of propylene, the observed dependence of rates on water molarity exhibited approximately second-order behavior at lower water ratio, which decreased to approximately first order at a higher water ratio (Fig. 4B and fig. S12). At lower propylene pressures, the water dependence showed more linear approximately first-order dependence in the entire water concentration range. For propylene, the rate showed first-order dependence on propylene activity at lower propylene pressures, but the dependence decreased at elevated propylene pressures (Fig. 4C and fig. S13).

To address the complexity arising from noninteger reaction orders and variations in orders with reactant concentrations, we implemented a multiparameter kinetic model and fitted it to the kinetic data collected over a wide range of experimental conditions. We initially hypothesized that surface-adsorbed hydroperoxo (OOH*), peroxo (OO*), or oxo (O*) species might serve as the reactive oxygen species for epoxidation. We then proposed various elementary steps and corresponding rates for each hypothesis (supplementary text S1). Given that acetonitrile is a less-effective proton acceptor than water, we suggested elementary steps in which two distinct water molecules play explicit roles in the reaction, one as a reactant and the other as a proton acceptor. Then, we employed kinetic modeling to deduce which intermediate would most likely react with propylene. This approach was viable because the reaction of different species (OOH*, OO*, and O*) with propylene generates distinct surface intermediates after epoxidation (OH*, O*, and *, respectively). By contrast, the evolution of O_2 invariably leaves vacant (*) surface sites. The goodness-of-fit of each model was evaluated by the root mean square error (RMSE) between the experimental data and the simulated data from the model, with the lowest value indicating the best-fit model.

Our experimental data best matched the mechanism suggesting OO* as the key intermediate for epoxidation, with an RMSE of 0.48 mA/cm^2. Diverse derivatives of this mechanism involving the OO* epoxidation intermediate are plausible, depending on whether a dual or single site is presumed for OO* and O* intermediates. We selected the model with the lowest RMSE as our representative mechanism (Fig. 4D), and the model provides a quantitative explanation of the data illustrated in Fig. 4, A to C. We also simulated surface coverage with the model (Fig. 4E and supplementary text S1). At higher propylene pressures where O* and OH* are abundant, the overall epoxidation rate would be largely determined by the rate of water oxidation to form OOH*. However, the comparable prevalence of different surface-oxygen intermediates underscores the necessity for a comprehensive kinetic model that does not assume a single dominant reactive intermediate and a rate-limiting step.

Kinetic isotope labeling and stilbene control experiments further support our hypothesis asserting OO* as the key intermediate in epoxidation. The use of deuterated water lowered the epoxidation rate (kinetic isotope effect value k_H/k_D = 1.8 ± 0.5; fig. S15 and table S10), and the FE remained similar. The difference observed in the epoxidation rate is consistent with the kinetically relevant water-activation steps involving O–H cleavages in our proposed mechanism. Moreover, our mechanism identifies OO* as the branching intermediate for both epoxide and O_2 evolution (Fig. 4D), providing an explanation for the marginal selectivity difference because neither of these pathways from OO* involves O–H cleavage. In addition, *cis*-stilbene was used as a probe substrate to help determine whether epoxidation proceeds through a concerted mechanism with OOH* or a stepwise pathway with OO* (*25*, *26*). *Cis*-stilbene (96%) epoxidation with PdPtO$_x$/C produced 23% *cis*-stilbene oxide and 77% *trans*-stilbene oxide, which suggests that alkene epoxidation over

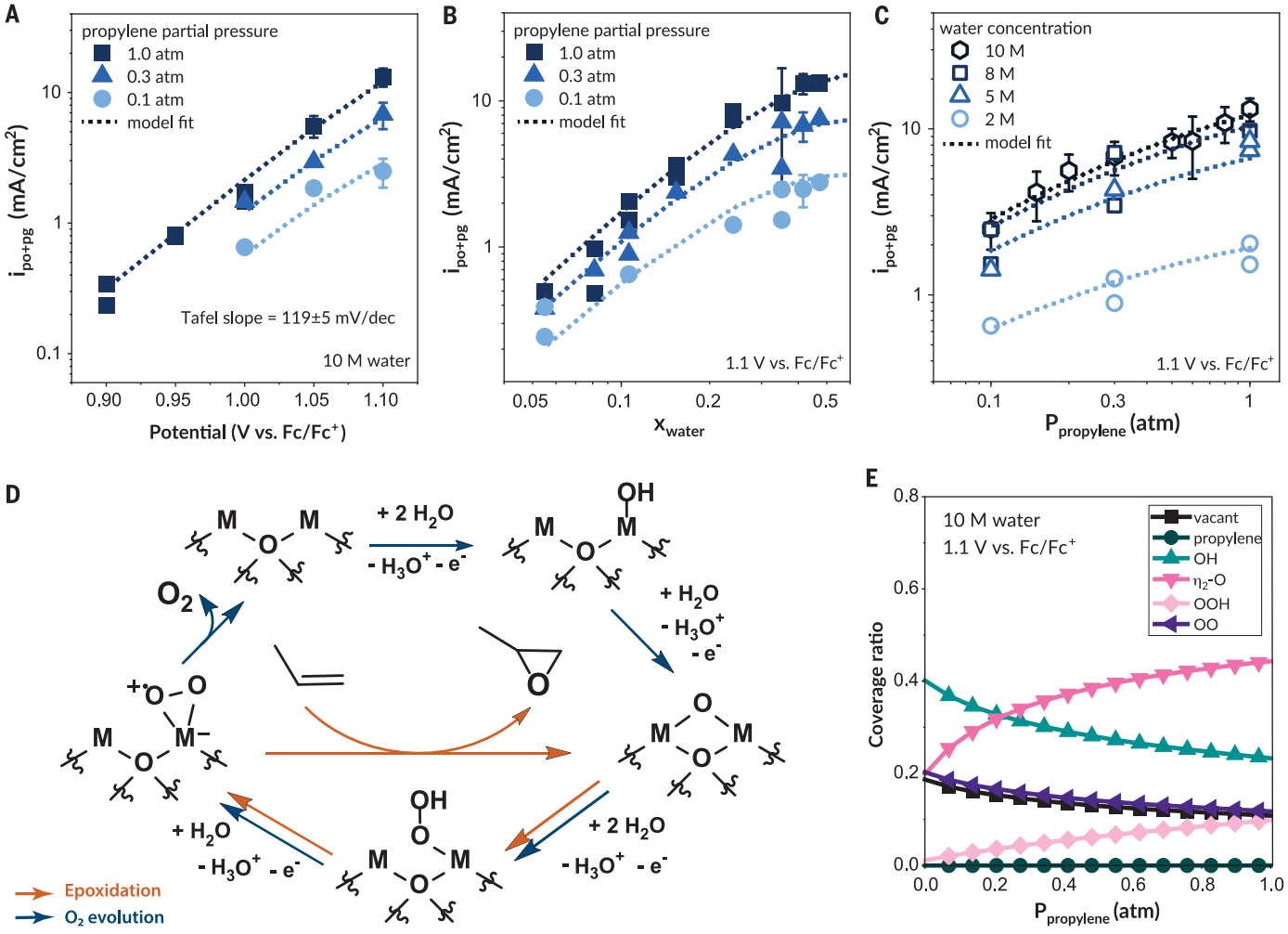

Fig. 4. Kinetic data on direct anodic epoxidation with $PdPtO_x$/C catalysts. (**A**) Anodic potential dependence of current density at 1 atm propylene in a 10 M water, 0.4 M tetrabutylammonium tetrafluoroborate ($TBABF_4$) acetonitrile solution. i_{po+pg}, partial current density toward PO and PG. (**B**) Water molar concentration dependences of propylene-epoxidation current density at different propylene partial pressures. (**C**) Propylene partial-pressure dependences of propylene-epoxidation current density at different water concentrations. (**D**) A putative reaction mechanism including the direct anodic-epoxidation and oxygen-evolution pathways. (**E**) Simulated propylene partial-pressure dependences of intermediate species coverage at 10 M water, 1.1 V versus Fc/Fc^+ condition. Potentials in this figure were 100% iR-compensated (i, current; R, resistance). Dotted lines in (A) through (C) represent best fit from kinetic model of proposed mechanism in (D) (more details are shown in supplementary text S1, Case 2d). Vertical error bars represent standard deviations from the mean of multiple replicates (n = 3) of the same experiment.

$PdPtO_x$/C occurs through a stepwise mechanism (fig. S16) with OO* reactive intermediates.

Correlation between alkene electrophilicity and epoxidation rate

Additional insights into direct anodic epoxidation on $PdPtO_x$/C were obtained from evaluating the correlation between the electrophilicity of alkene substrates and the epoxidation rate. Previous studies on thermochemical epoxidation suggest that either electrophilic (*27*–*29*) or nucleophilic (*30*, *31*) epoxidation can be a reasonable reaction pathway for electrochemical propylene epoxidation on late-transition metal catalysts (supplementary text S2). By understanding the electronic nature of the oxygen transfer during the reaction, we can enhance our understanding of the mechanism and guide future catalyst development.

The global electrophilicity index (ω) can be calculated by taking the square of alkene chemical potential divided by chemical hardness and is expressed in units of energy (*32*, *33*). A higher value of ω indicates that the molecule is more electrophilic. Furthermore, the Fukui functions can be used to determine the local reactivity of each atom in a molecule by predicting the redistribution of electron density during electrophilic, nucleophilic, and radical attacks. The local electrophilicity (ω^-) at each atom center can be obtained by multiplying the global electrophilicity by the value of the Fukui function for the removal of an electron.

The average ω^- of the vinyl carbons as a substrate-based descriptor was assessed against the epoxidation rates of a wide range of alkene substrates. A total of 11 distinct aliphatic alkenes with various structures and functional groups were selected, with ω^- values ranging from 12 to 44 kJ/mol. To ensure consistent reactant chemical potential across different substrates, the gaseous substrates were fed until saturation, and the liquid substrates were added to the electrolyte near the phase-separation point, corresponding to ~0.2 M substrate for a 0.11 M tetrabutylammonium tetrafluoroborate ($TBABF_4$), 10 M water in acetonitrile (table S11). The substrates were tested at the same potential referenced to the ferrocene redox couple (1.05 V versus Fc/Fc^+).

A negative correlation between the logarithm of rate and the alkene electrophilicity was observed, with more nucleophilic alkenes displaying higher reactivity toward epoxidation (Fig. 5). The results suggest that the epoxidation may proceed through an electrophilic

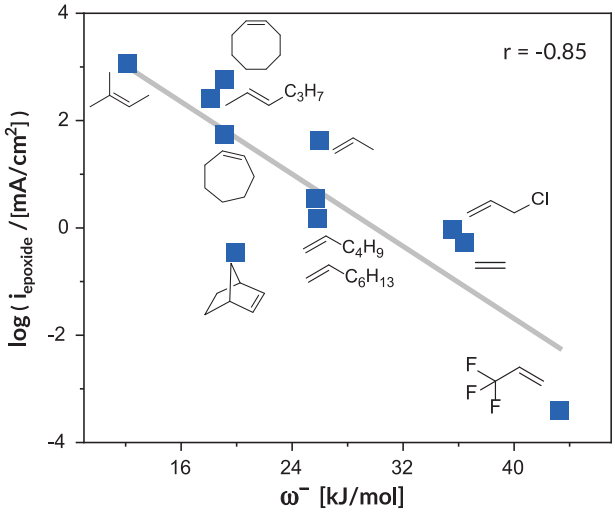

Fig. 5. Correlation between the alkene electrophilicity index and the direct anodic-epoxidation rate. Pearson correlation coefficient (*r*) value = −0.85.

attack by oxygen species and that the energy barriers to this attack are lower for more nucleophilic alkenes. Furthermore, the correlation suggests that a frontier-orbital interaction between the lowest unoccupied molecular orbital (LUMO) of the oxygen species and the highest occupied molecular orbital (HOMO) of the alkene modulates the reactivity.

Electrolyte choice and the effect of solvent medium on the reaction kinetics

The successful operation of direct epoxidation through water activation hinges on whether the electrolyte system is compatible with a particular combination of catalyst and alkene substrate. Water-acetonitrile blended electrolytes were used to investigate the epoxidation of various alkene substrates because the acetonitrile cosolvent enhances the solubility of hydrophobic alkene substrates in the water-rich phase. However, the use of an organic solvent can lead to an increase in the ohmic resistance throughout the electrolyte (fig. S4). The use of water alone as the solvent for the electrolyte, without an organic cosolvent, would be ideal because water is required as a reactant and can effectively solvate electrolyte ions, minimizing the ohmic resistance of the overall electrolyte. For gaseous substrates that are sparingly soluble in water, such as propylene, gas-diffusion electrodes (GDEs) could be used to reduce the distance that reactant gases must diffuse through the electrolyte to reach the catalyst, and therefore, aqueous electrolytes would be sufficient for epoxide production. Indeed, the $PdPtO_x$/C catalyst showed ~60% FE toward propylene epoxidation at 1.65 V versus standard hydrogen electrode (SHE) in a sodium phosphate aqueous electrolyte when incorporated into a carbon-paper GDE with Nafion binder (Fig. 1E and fig. S4). Adding the ionomer onto the electrode was critical to achieve epoxidation performance commensurate with water-acetonitrile electrolytes because the hydrophobic backbone of the ionomer generates partially wetted channels that are effective for transport of the reactant gases to the catalyst.

The microenvironment of electrolytes also affects the conversion of epoxides into glycols. A noticeable amount of PG was observed in the aqueous propylene epoxidation (~10% FE), higher than that observed in the blended water-acetonitrile electrolyte. Furthermore, using 0.1 M $HClO_4$ or any acidic electrolyte results in the exclusive formation of PG, with no detected PO (table S1). Because epoxides are known to undergo acid-catalyzed hydrolysis to afford glycols, it is imperative to find a pH regime in which hydrolysis is minimized to ensure high selectivity toward the product of interest in aqueous electrolytes. The reaction rates of PO to PG in aqueous electrolytes with pH 4 to 7 were measured with ^{1}H-NMR: The hydrolysis of PO to generate PG was found to be faster in the pH 4 buffer solution, with almost 40% consumption of PO after 7 hours, whereas the hydrolysis in less-acidic solutions, at pH 5 to 7, was largely suppressed, with less than around 10% PO to PG conversion (fig. S18). Thus, maintaining a near-neutral pH in the aqueous electrolyte is essential to optimize PO production.

The practical industrial operation of this system will likely require the use of a membrane-electrode assembly (MEA) resembling a water electrolyzer with humidified propylene gas fed to the anode. The MEA is advantageous for minimizing ohmic loss and separating PO from liquid electrolytes. However, our analysis on the influence of pH on the PO hydrolysis rate suggests that minimizing the interfacial pH gradient at the anode would be the key challenge for maximizing PO production over PG in MEAs operated at high current densities.

As long as the issues of mass-transport limitation and hydrolysis of PO are addressed, mechanistic insights on propylene epoxidation obtained in water-acetonitrile electrolyte may be extended to aqueous systems. The investigation on water activity in water-acetonitrile electrolyte suggests that the aqueous electrolyte may be viewed as an extreme case of the water-acetonitrile electrolyte with the water molar ratio approaching unity. In the water-acetonitrile electrolyte system, positive deviation from Raoult's law (fig. S17) indicates that the water in this electrolyte prefers self-interactions over mixing, meaning that the activity coefficient of water in this case is greater than unity ($\gamma_{water} > 1$) and that it approaches unity with increasing water concentration. The comparison between the rate order with respect to water activity and water concentration provides information about the activity coefficient of the transition state ($\gamma_{\ddagger}$) as well (supplementary text S4). At lower water concentrations (1 to 5 M), the propylene-epoxidation rate showed approximately fourth-order dependence on water activity, whereas approximately second-order dependence on water molar ratio was observed. The second-order dependence is consistent with our hypothesis that the predominant rate-determining step leading to the formation of OOH* involves a first water molecule that is a reactant and a second water molecule that is a proton acceptor. The abnormally high apparent fourth-order dependence on water activity suggests that the stabilization of the transition state may be achieved by augmenting the water content. However, approximately second-order dependences in both water activity and concentration were observed at higher water concentrations (5 to 12 M). This can be rationalized if $\gamma_{\ddagger}$ scales with γ_{water} at low water concentrations but remains relatively unchanged at higher water concentrations. This hypothesis aligns with our chemical intuition: Once a sufficient quantity of water is present around the transition state, adding more water does not substantially alter the near–transition state chemical environment. Therefore, once the water concentration exceeds 5 M in acetonitrile, the chemical environment at the active site should be akin to that of an aqueous electrolyte. In this case, the transition from water-acetonitrile electrolyte to aqueous electrolyte may be a simple extrapolation of water molar ratio to one, without a discontinuous change in the solvent properties. This interpretation is supported by the measured reaction rates in aqueous electrolytes that is consistent with the predictions from the mechanistic model derived from kinetic studies in water-acetonitrile electrolytes (fig. S12).

Collectively, the results from multiple orthogonal analyses provide a comprehensive understanding of the mechanism of electrochemical epoxidation on $PdPtO_x$/C. Our findings are consistent with a mechanistic hypothesis that OO* is the key species involved in the electrophilic epoxidation of propylene. The PdO

crystal structure embedding Pt(II) species was found to be effective for catalyzing direct anodic epoxidation, suggesting that other materials with similar structures and stronger inductive effects on Pt may also produce effective catalysts by promoting more electrophilic epoxidation pathways. Additionally, we discovered through fundamental kinetic analysis that the identity of reactive oxygen species may vary between catalysts. For instance, the proposed reactive oxygen species for epoxidation on $PdPtO_x$/C and MnO_x-based catalysts (*7*, *8*) are OO* and O*, respectively. Developing approaches to stabilize OO* may enhance epoxidation on noble metals while avoiding oxygen evolution. Our work contributes toward advancing the sustainable synthesis of epoxides, which currently have substantial energy and environmental footprints. The molecular-level understanding of direct anodic epoxidation obtained from this study may have implications for other electrocatalytic oxygen-atom transfer reactions driven by water-activation intermediates.

REFERENCES AND NOTES

1. M. W. Allsopp, G. Vianello, *Ullmann's Encyclopedia of Industrial Chemistry* – Wiley Online Library (Wiley, 2012); https://onlinelibrary.wiley.com/doi/book/10.1002/14356007.
2. S. J. Khatib, S. T. Oyama, *Catal. Rev. Sci. Eng.* **57**, 306–344 (2015).
3. J. A. M. Leduc, "Electrochemical Process for the Production of Organic Oxides," US Patent 3,288,692 (1966).
4. W. R. Leow *et al*., *Science* **368**, 1228–1233 (2020).
5. M. Chung, K. Jin, J. S. Zeng, K. Manthiram, *ACS Catal.* **10**, 14015–14023 (2020).
6. J. A. M. Le Duc, "Electrolytic Production of Olefine Oxides," US Patent 3,427,235 (1969).
7. M. Chung, K. Jin, J. S. Zeng, T. N. Ton, K. Manthiram, *J. Am. Chem. Soc.* **144**, 17416–17422 (2022).
8. K. Jin *et al*., *J. Am. Chem. Soc.* **141**, 6413–6418 (2019).
9. X. C. Liu *et al*., *J. Am. Chem. Soc.* **144**, 20895–20902 (2022).
10. A. Winiwarter *et al*., *Energy Environ. Sci.* **12**, 1055–1067 (2019).
11. R. P. H. Jong, E. Dubbelman, G. Mul, *J. Catal.* **416**, 18–28 (2022).
12. S. Koroidov *et al*., *Catal. Sci. Technol.* **11**, 3347–3352 (2021).
13. K. Otsuka, T. Ushiyama, I. Yamanaka, K. Ebitani, *J. Catal.* **157**, 450–460 (1995).
14. S. Iguchi, M. Kataoka, R. Hoshino, I. Yamanaka, *Catal. Sci. Technol.* **12**, 469–473 (2022).
15. I. Yamanaka, K. Sato, K. Otsuka, *Electrochem. Solid-State Lett.* **2**, 131–132 (1999).
16. L. L. Holbrook, H. Wise, *J. Catal.* **38**, 294–298 (1975).
17. J. Ke *et al*., *Nat. Commun.* **13**, 932 (2022).
18. H. Li, C. S. Abraham, M. Anand, A. Cao, J. K. Nørskov, *J. Phys. Chem. Lett.* **13**, 2057–2063 (2022).
19. M. Chen, L. D. Schmidt, *J. Catal.* **56**, 198–218 (1979).
20. C. Carrillo *et al*., *J. Phys. Chem. Lett.* **5**, 2089–2093 (2014).
21. P. N. Plessow, F. Abild-Pedersen, *ACS Catal.* **6**, 7098–7108 (2016).
22. E. D. Goodman *et al*., *J. Chem. Phys.* **151**, 154703 (2019).
23. A. Aitbekova *et al*., *Nat. Mater.* **21**, 1290–1297 (2022).
24. D. Gao *et al*., *J. Am. Chem. Soc.* **137**, 4288–4291 (2015).
25. D. T. Bregante, P. Priyadarshini, D. W. Flaherty, *J. Catal.* **348**, 75–89 (2017).
26. C. K. Sams, K. A. Jørgensen, S. V. Lindeman, J. Songstad, *Acta Chem. Scand.* **49**, 839–847 (1995).
27. C. Kim, T. G. Traylor, C. L. Perrin, *J. Am. Chem. Soc.* **120**, 9513–9516 (1998).
28. X. Yang *et al*., *Angew. Chem. Int. Ed.* **54**, 11946–11951 (2015).
29. Y. Lei *et al*., *Science* **328**, 224–228 (2010).
30. A. R. Chianese, S. J. Lee, M. R. Gagné, *Angew. Chem. Int. Ed.* **46**, 4042–4059 (2007).
31. A. Zanardo, F. Pinna, R. A. Michelin, G. Strukul, *Inorg. Chem.* **27**, 1966–1973 (1988).
32. F. De Vleeschouwer, V. Van Speybroeck, M. Waroquier, P. Geerlings, F. De Proft, *Org. Lett.* **9**, 2721–2724 (2007).
33. R. Pal, P. K. Chattaraj, *J. Comput. Chem.* **44**, 278–297 (2023).
34. M. Chung *et al*., Direct propylene epoxidation via water activation over Pd-Pt electrocatalysts, Version 3, Dryad (2024); https://doi.org/10.5061/dryad.s7h44j1dd.

ACKNOWLEDGMENTS

We are grateful to S. Ehrlich, L. Ma, E. Stavitski, and D. Leshchev for their help in operating XAS experiments. We also appreciate A. Penn for taking high-resolution energy dispersive spectroscopy mapping of catalysts. **Funding:** This research was supported by the US Department of Energy (DOE) Office of Science, Office of Basic Energy Sciences, Catalysis Science Program, award no. DE-SC0023207. K.M. gratefully acknowledges the support of the Sloan Foundation. This research used resources of the National Synchrotron Light Source II, a US DOE Office of Science User Facility operated by Brookhaven National Laboratory under contract no. DE-SC0012704. **Author contributions:** Conceptualization: M.C. and K.M. Methodology: M.C. Investigation: M.C., J.H.M., and J.S.A. Validation: M.C. and J.S.A. Visualization: M.C. Funding acquisition: K.M. Project administration: M.C. and K.M. Supervision: K.M. and Y.R.-L. Writing – original draft: M.C. Writing – review and editing: M.C., J.H.M., J.S.A., C.J., Y.R.-L., and K.M. **Competing interests:** M.C. and K.M. have filed a provisional patent application (no. 63/544,664) regarding the design of catalysts and electrodes. **Data and materials availability:** There are no restrictions on materials. All data needed to evaluate the conclusions in the paper are present in the paper or the supplementary materials. Tabular data underlying the figures are deposited in the Dryad data repository (*34*).

SUPPLEMENTARY MATERIALS

science.org/doi/10.1126/science.adh4355
Materials and Methods
Supplementary Text
Figs. S1 to S25
Tables S1 to S12
References (*35*–*39*)

Submitted 4 March 2023; resubmitted 12 September 2023
Accepted 29 November 2023
10.1126/science.adh4355

Direct propylene epoxidation via water activation over Pd-Pt electrocatalysts

Minju Chung, Joseph H. Maalouf, Jason S. Adams, Chenyu Jiang, Yuriy Román-Leshkov, and Karthish Manthiram

Science **383** (6678), . DOI: 10.1126/science.adh4355

Editor's summary

Propylene oxide is produced at massive scale using dangerous and corrosive oxidants. A potentially safer method uses electrochemistry to oxidize propylene with water, but catalyst stability is a persistent challenge. Chung *et al*. report that by alloying palladium with platinum, they could generate an electrocatalyst that delivered >60% Faradaic efficiency toward propylene epoxidation by water oxidation. Initially focusing on acetonitrile as a cosolvent, the authors went on to explore purely aqueous media and discuss the prospects of improving propylene throughput in the face of low solubility. —JSY